Thermofield-based chain-mapping approach for open quantum systems

Inés de Vega[1] and Mari-Carmen Bañuls[2]

[1]*Department of Physics and Arnold Sommerfeld Center for Theoretical Physics, Ludwig-Maximilians-University Munich, 80333 Munich, Germany*

[2]*Max-Planck-Institut für Quantenoptik, Hans-Kopfermann-Strasse 1, 85748 Garching, Germany*

(Received 4 May 2015; published 20 November 2015)

We consider a thermofield approach to analyze the evolution of an open quantum system coupled to an environment at finite temperature. In this approach, the finite-temperature environment is exactly mapped onto two virtual environments at zero temperature. These two environments are then unitarily transformed into two different chains of oscillators, leading to a one-dimensional structure that can be numerically studied using tensor network techniques. Compared to previous approaches using a single chain mapping, our strategy offers the advantage of an exact description of the initial state at arbitrary temperatures, which results in a gain in computational efficiency and a reduced truncation error.

DOI: 10.1103/PhysRevA.92.052116 PACS number(s): 03.65.Yz, 03.70.+k, 03.65.Ca

I. INTRODUCTION

In the past few decades, many different techniques have been developed to analyze the dynamics of quantum systems coupled to an environment, i.e., open quantum systems (OQSs). Some of these are based on deriving a master equation (ME), which evolves the reduced density operator of the OQS by tracing out the environment degrees of freedom [1,2], and some others are based on the stochastic Schrödinger equations (SSEs), which evolve the OQS wave function conditioned by a continuous [3–5] or discrete [6,7] stochastic process. Both approaches are suitable for weak system-environment couplings, which generally lead to a large separation between system and environment time scales. Although such a large separation often occurs in quantum optics, it does not necessarily occur in other scenarios, such as soft- or condensed-matter systems, or in quantum biology. In these situations, other approaches are more appropriate, such as the path-integral Monte Carlo method [8], which in some parameter regimes is nevertheless hindered by the sign problem, potentially affecting the convergence of the method at relatively short times (see, for instance, [9]).

An alternative is to solve the total system dynamics with exact diagonalization methods, but this is difficult due to the large number of degrees of freedom in the environment. Hence, a wise selection of the relevant states of the full system is of primary importance, and this can be done, for instance, by discarding states with low probability, as in the density matrix approach [10] (closely related to the density-matrix renormalization group), or by considering relevant only those states generated during the evolution, as done in the variational approach [11,12].

Apart from exact diagonalization, the total system dynamics can be solved based on performing first a unitary transformation of the environment that *maps* it onto a one-dimensional structure. The numerical renormalization-group approach [13–18], for instance, is based on (logarithmic) coarse graining of the continuous environment spectral function in energy space. The resulting discretized environment can then be mapped onto a semi-infinite tight-binding chain [19] with exponentially decreasing couplings. As proposed in [20–22] (see also [23] for a discussion), the mapping can also be performed analytically without previous discretization of the environment. Even when the couplings do not decay exponentially, it is typically possible to describe the system dynamics until its decay or relaxation time using a truncated chain of finite length. The total system can now be modeled as a matrix product state (MPS), and it is then possible to use tensor network techniques to simulate the unitary evolution of the total system [24–27]. The approach can also deal with an environment at finite temperature, using matrix product operators [28,29].

In this paper, we present an alternative formulation of the latter method to calculate MPS dynamics with initial thermal states. Our method is based on the thermofield approach proposed in [30–32] (see [33] for an excellent review). In this approach, the environmental Hilbert space is mirrored or doubled, and then a thermal Bogoliubov transformation is performed. As a result, the real environment in a thermal state is transformed into two virtual environments in a vacuum state [see Fig. 1(b)], known in the literature as the thermofield vacuum. The expectation value of any operator of the real environment in the thermofield vacuum coincides with its expectation value in the thermal state. The only excitations appearing in the environment will be those that are dynamically created through the interaction, and the dynamics of the resulting transformed system can be simulated using MPS.

The thermofield approach has been considered in the framework of SSEs of OQSs (see, for instance, [3,4]), but most of its applications are in the context of quantum field theory and general relativity [34,35].

II. THERMOFIELD DYNAMICS

Let us consider an environment of harmonic oscillators, with annihilation (creation) operators b_k ($b_k^\dagger$) and frequencies ω_k, to which the OQS couples with strengths g_k. The complete Hamiltonian can be written as

$$H_{\rm tot} = H_S + H_B + \sum_k g_k (L^\dagger b_k + b_k^\dagger L), \tag{1}$$

where H_S is the Hamiltonian of the OQS, $H_B = \sum_k \omega_k b_k^\dagger b_k$, and L is the coupling operator acting on the OQS Hilbert

space. We can introduce an auxiliary, decoupled environment, characterized by annihilation (creation) operators c_k ($c_k^\dagger$), and write the total Hamiltonian as

$$\hat{H}_{\rm tot} = H_{\rm tot} - \sum_k \omega_k c_k^\dagger c_k. \tag{2}$$

Assuming now that both environments are initially in a thermal state at inverse temperature β, we apply a thermal Bogoliubov transformation,

$$\begin{aligned} a_{1k} &= e^{-iG} b_k e^{iG} = \cosh(\theta_k) b_k - \sinh(\theta_k) c_k^\dagger, \\ a_{2k} &= e^{-iG} c_k e^{iG} = \cosh(\theta_k) c_k - \sinh(\theta_k) b_k^\dagger. \end{aligned} \tag{3}$$

Here, $G = i\sum_k \theta_k (b_k^\dagger c_k^\dagger - c_k b_k)$, with θ_k being a function of the temperature such that

$$\begin{aligned} \cosh(\theta_k) &= \sqrt{1+n_k}, \\ \sinh(\theta_k) &= \sqrt{n_k}, \end{aligned} \tag{4}$$

where $n_k = 1/(e^{\beta\omega_k} - 1)$ is the number of excitations in mode k. In terms of these new modes,

$$\begin{aligned} \tilde{H}_{\rm tot} = H_S + \sum_k \omega_k (a_{1k}^\dagger a_{1k} - a_{2k}^\dagger a_{2k}) + \sum_k g_{1k}(L^\dagger a_{1k} + a_{1k}^\dagger L) \\ + \sum_k g_{2k}(L a_{2k} + a_{2k}^\dagger L^\dagger), \end{aligned} \tag{5}$$

where $g_{1k} = g_k \cosh(\theta_k)$ and $g_{2k} = g_k \sinh(\theta_k)$. The thermal vacuum can be written in terms of the vacuum for b_k and c_k modes, $|\Omega_0\rangle$, as

$$|\Omega\rangle = e^{-iG}|\Omega_0\rangle. \tag{6}$$

The thermal vacuum can be written in alternative ways that further enlighten its physical meaning: First, it can be written as

$$|\Omega\rangle = e^{-S/2} e^{\sum_k b_k^\dagger c_k^\dagger} |\Omega_0\rangle, \tag{7}$$

in terms of the quantity $S = -\sum_k [b_k^\dagger b_k \log\sinh^2(\theta_k) - b_k b_k^\dagger \log\cosh^2(\theta_k)]$, which can be interpreted as the entropy operator for the physical (original) environment [33] since the thermofield vacuum is the state that minimizes the thermodynamic potential $\langle\Omega|(-\frac{1}{\beta}S + H)|\Omega\rangle$. Second, up to normalization, we can write

$$|\Omega\rangle \propto e^{-\beta H_B/2}|I\rangle, \tag{8}$$

with $|I\rangle = \sum_n |n\rangle_b |n\rangle_c$ being the maximally entangled state between the real and the auxiliary environments, defined in terms of their energy eigenstates, $|n\rangle_b$, $|n\rangle_c$. The thermal state of the original environment is thus $\rho_B = {\rm Tr}_{\rm aux}[|\Omega\rangle\langle\Omega|]$, and it can be approximated by a matrix product operator (MPO) by evolving the maximally entangled state in imaginary time [28,29]. In contrast, the present approach is based on directly calculating the dynamics of the whole system under the Hamiltonian (5), using the thermofield vacuum as a (pure) initial state for both reservoirs. Although this state is annihilated by a_{1k} and a_{2k}, the number of physical particles has a nonvanishing expectation value $n_k = \langle\Omega|b_k^\dagger b_k|\Omega\rangle = \sinh^2(\theta_k)$. Hence, solving the dynamics of the initial problem (1) with an initial condition $\rho_0^{\rm tot} = \rho_0^S \otimes \rho_B$, with ρ_0^S being the initial state of the system, is equivalent to solving the dynamics with (5) but considering $\rho_0^{\rm tot} = \rho_0^S \otimes |\Omega\rangle\langle\Omega|$ [see Figs. 1(a) and 1(b), respectively].

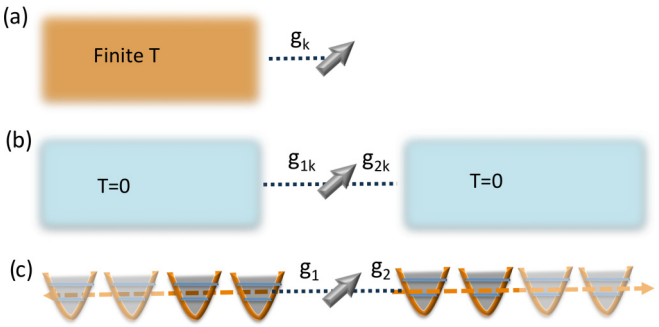

FIG. 1. (Color online) (a) The initial problem described with (1) of an OQS coupled to a harmonic oscillator reservoir at finite temperature. (b) The thermofield-transformed problem (2), in which the finite temperature of the reservoir is encoded in two different reservoirs at zero temperature. (c) The chain representation of the latter.

We have described in detail the thermofield transformation for bosonic environments, but a similar Bogoliubov transformation can be proposed for fermionic reservoirs. In that case [33] we have

$$\begin{aligned} a_{1k} &= e^{-iG} b_k e^{iG} = \cos(\theta_k) b_k - \sin(\theta_k) c_k^\dagger, \\ a_{2k} &= e^{-iG} c_k e^{iG} = \cos(\theta_k) c_k + \sin(\theta_k) b_k^\dagger. \end{aligned} \tag{9}$$

With this transformation, the Hamiltonian (2) is transformed into (5).

III. CHAIN REPRESENTATION

The Hamiltonian (5) represents an OQS interacting with two independent environments, which have operators a_{1k} and a_{2k}, respectively. The whole problem can be mapped into a one-dimensional structure with the schematic form in Fig. 1(c). In general, the environment oscillators in (1) form a quasicontinuum, so that the Hamiltonian (1) can be rewritten as

$$\begin{aligned} H = H_S + \int_0^1 dk g(k)[b(k)L^\dagger + L b(k)^\dagger] \\ + \int_0^1 dk \omega(k) b(k)^\dagger b(k), \end{aligned} \tag{10}$$

where $b(k)$ [$b^\dagger(k)$] is the continuous counterpart of b_k ($b_k^\dagger$), $g(k)$ is the continuous counterpart of the coupling strength g_k, and $\omega(k)$ is the continuous counterpart of the dispersion ω_k. In addition, we have rescaled the integrals, such that $\omega(1) = \omega_{\rm max}$, i.e., the frequency cutoff of the environment. When the environment is in a Gaussian state, $\omega(k)$ and $g(k)$ enter the description of the OQS only through the spectral density, $J(\omega(k)) = g^2(k) D(\omega(k))$, where $D(\omega(k)) = |\partial\omega(k)/\partial k|^{-1}$ is the photonic density of states (DOS).

One can reproduce the same spectral density by introducing a new dispersion $\hat{\omega}(k) = \omega_0 k$ (with ω_0 being an arbitrary constant that may be taken as 1), such that $D(\hat{\omega(k)}) = \omega_0$, and a new coupling $\hat{g}(k)$, such that $\hat{g}(k) = \sqrt{J(\omega(k))}$. In terms of these new quantities, the continuum representation of (5)

reads

$$\tilde{H}_{\rm tot} = H_S + \int_0^1 dk k(a_{1k}^\dagger a_{1k} - a_{2k}^\dagger a_{2k}) + \int_0^1 dk[\hat{g}_1(k)(L^\dagger a_{1k} + a_{1k}^\dagger L) + \hat{g}_2(k)(La_{2k} + a_{2k}^\dagger L^\dagger)].$$

Thus, the spectral densities of each of the two new (transformed) environments are

$$\begin{aligned} J_1(k) &= \hat{g}_1^2(k) = \sum_k [1 + n(\hat{\omega}(k))] J(\hat{\omega}(k)), \\ J_2(k) &= \hat{g}_2^2(k) = n(\hat{\omega}(k)) J(\hat{\omega}(k)), \end{aligned} \tag{11}$$

where we have defined $n(\hat{\omega}(k))$ as the number of excitations in the mode with frequency $\hat{\omega}(k)$, i.e., the continuous version of the Planck distribution n_k. Then, using the unitary transformation discussed in [20,21], new bosonic operators B_n and C_n can be defined for each reservoir, such that

$$a_{1k} = \sum_n U_{1n}(k) B_n, \quad a_{2k} = \sum_n U_{2n}(k) C_n, \tag{12}$$

where $U_{jn}(k) = g_j(k)\pi_{jn}(k)/\rho_{nj}$ $(j = 1,2)$. Here, $\pi_{jn}(k)$ are monic orthogonal polynomials that obey

$$\int_0^1 dk J_j(k) \pi_{j,n}(k) \pi_{j,m}(k) = \rho_{nj}^2 \delta_{nm}, \tag{13}$$

with $\rho_{nj}^2 = \int_0^1 dk J_j(k) \pi_{j,n}^2(k)$ [21,22]. Hence, the proposed transformation is also orthogonal, $\int dk U_{jn}^* U_{jm} = \delta_{nm}$. The transformed Hamiltonian can be written as $\tilde{H}_{\rm tot}^{\rm ch} = H_S + H_B^{\rm ch} + \tilde{H}_{\rm int}^{\rm ch}$, with the interaction of the system with the first harmonic oscillator of each chain given by

$$\tilde{H}_{\rm int}^{\rm ch} = g_1(L^\dagger B_0 + B_0^\dagger L) + g_2(LC_0 + C_0^\dagger L^\dagger), \tag{14}$$

with $g_j = \rho_{j0}$, and the Hamiltonian of the two chains given by

$$\tilde{H}_B^{\rm ch} = \sum_{n=0,\ldots,M} (\alpha_{1,n} B_n^\dagger B_n - \alpha_{2,n} C_n^\dagger C_n + \sqrt{\beta_{1,n+1}} B_{n+1}^\dagger B_n - \sqrt{\beta_{2,n+1}} C_{n+1}^\dagger C_n + \text{H.c.}). \tag{15}$$

In order to perform the mapping, the recurrence relation of the orthogonal polynomials have been used, namely,

$$\pi_{j,n+1}(k) = (k - \alpha_{j,n})\pi_{j,n}(k) - \beta_{j,n}\pi_{j,n-1}(k), \tag{16}$$

with $\pi_{j,-1}(k) = 0$, $\pi_{j,0}(k) = 1$, and $n = 0, \ldots, M-1$. The coefficients of this recurrence, $\alpha_{j,n}$ and $\beta_{j,n}$, can be obtained with standard numerical routines [36]. Hence, the resulting Hamiltonian describes two tight-binding chains to which the system is coupled. The thermofield vacuum is also annihilated by the new modes B_n and C_n, so that the dynamics of the whole system can be simulated using MPS time-evolution methods from an initial state with zero occupancy of each of these modes (see the Appendix for details on the numerical method). Note that a similar mapping can be applied in the case of a finite discrete environment by means of a standard Lanczos tridiagonalization.

The thermofield approach presented here provides several advantages with respect to applying previous strategies [20–22] to a bath at finite temperature. First, the thermal state of the bath at arbitrary temperature corresponds in our representation to a vacuum state (i.e., the thermal vacuum), which therefore does not contain any initial excitation, which gives rise to a potentially better scaling of the local basis dimension needed in the MPS formulation. Second, this thermal vacuum is a product state, and therefore, it has an exact MPS representation with bond dimension $D = 1$. In terms of the transformed set of modes for the chain representation proposed in [20–22], the thermal state is a global operator, for which a MPO approximation needs to be computed, using a finite bond dimension, which introduces both a computational overhead and an additional source of error.

In addition, the method provides new physical insight into the problem. In particular, the difference in the total occupation between the two chains gives the deviation of the environment state from its thermal distribution, namely,

$$\begin{aligned} N(t) &= \sum_k (\langle\Omega|b_k^\dagger(t) b_k(t)|\Omega\rangle - \langle\Omega|c_k^\dagger(t) c_k(t)|\Omega\rangle) \\ &= N_1(t) - N_2(t), \end{aligned} \tag{17}$$

where the auxiliary reservoir remains always in the thermal state, such that $\langle c_k^\dagger(t) c_k(t)\rangle = n_k$ at all times, and we have defined

$$\begin{aligned} N_1(t) &= \sum_n \langle\Omega_0|B_n^\dagger(t) B_n(t)|\Omega_0\rangle \\ &= \sum_k \langle\Omega_0|a_{1k}^\dagger(t) a_{1k}(t)|\Omega_0\rangle, \\ N_2(t) &= \sum_n \langle\Omega_0|C_n^\dagger(t) C_n(t)|\Omega_0\rangle \\ &= \sum_k \langle\Omega_0|a_{2k}^\dagger(t) a_{2k}(t)|\Omega_0\rangle. \end{aligned} \tag{18}$$

Thus, the larger the population imbalance is between the two transformed environments, the larger the deviation from the initial thermal state is. In this regard, note that $N(t)$ can acquire negative values when the open system absorbs energy from the environment.

IV. NUMERICAL EXAMPLES

In the following, we present numerical results to illustrate this approach in different examples. The numerical errors in our simulations arise from the various truncation parameters and can thus be controlled by varying them. In the first place, the finite bond dimension D of the MPS representing the time-dependent states introduces a truncation error. Its magnitude can be estimated by comparing results with increasing values of D. The chain representation for the environments we study in this section is, in principle, semi-infinite. In practice, nevertheless, one can work with a finite chain, thus truncating also the number of environmental modes included in the evolution. Again, the effect of this truncation can be controlled by repeating the simulation with longer chains. Finally, to deal with bosonic environments in the MPS formalism, it is necessary to approximate them with finite-dimensional Hilbert spaces. Although more accurate methods exist [37], a standard technique is to simply truncate the occupation number per bosonic mode to a certain maximum value.

In our simulations, we vary the values of the truncation parameters described above until the variations induced by them are negligible compared to the effects we wish to study, and we present the results already converged in that way.

A. A spin in a bosonic field

Let us consider a spin-1/2 system coupled to a bosonic environment with spectral density given by the Caldeira and Leggett model [38,39],

$$J(\omega) = \eta \omega^s e^{-\omega/\omega_c}, \tag{19}$$

with $0 < s < 1$ in the *sub-Ohmic* case and $s > 1$ in the *super-Ohmic*. Roughly speaking, the constant η gives the coupling strength between the system and environment. The exponential factor in (19) provides a smooth cutoff for the spectral density, modulated by a frequency cutoff ω_c. This general model provides a good approximation for spectral densities appearing in many different problems, like an impurity in a photonic crystal [40,41], quantum impurity models [42], and solid-state devices at low temperatures such as superconducting qubits [43], quantum dots [44], and nanomechanical oscillators [45], to name just a few examples.

In the following, we shall consider natural units in which $\hbar = 1$, and the Boltzmann constant $k_B = 1$. As a first check we consider a solvable example, with $H_S = \frac{1}{2}\omega_S \sigma_z$ and $L = \sigma_z$ in (1). Here, ω_S is the system rotating frequency, and σ_j $(j = x,y,z)$ are the standard Pauli matrices describing spin-1/2 systems. For an initial state $|\psi_0\rangle = a|0\rangle + b|1\rangle$, the expectation value of any system operator A can be analytically calculated [46],

$$\langle A(t)\rangle = e^{-2\phi_t}\{|a|^2 e^{i\omega_S t} + |b|^2 e^{-i\omega_S t}\}, \tag{20}$$

with $\phi_t = \int_0^t d\tau \int_0^\tau ds \mathrm{Re}[\alpha_T(\tau - s)]$, $\alpha_T(t) = \sum_k g_k^2[\coth(\frac{\omega_k \beta}{2})\cos(\omega_k t) - i\sin(\omega_k t)]$.

To simulate the problem numerically using MPS we need to truncate the maximum occupation number of the bosonic modes and the length of the chains corresponding to the transformed environment. We compare the numerical solution to the exact one for $A = \sigma_x$ in Fig. 2 and observe very good agreement for all considered spectral densities, couplings, and temperatures for a relatively small bond dimension and length of each chain M.

In the following, we consider a problem that is not exactly solvable by choosing $L = \sigma_x$ and compare the solutions of our method with those corresponding to a master equation up to second order in the system-environment coupling parameter g,

$$\begin{aligned}\frac{d\rho_s(t)}{dt} = &-i[H_S, \rho_s(t)] + \int_0^t d\tau \alpha_2^*(t-\tau)[L^\dagger, \rho_s(t)L(\tau - t)] \\ &+ \int_0^t d\tau \alpha_2(t-\tau)[L^\dagger(\tau - t)\rho_s(t), L] \\ &+ \int_0^t d\tau \alpha_1(t-\tau)[L(\tau - t)\rho_s(t), L^\dagger] \\ &+ \int_0^t d\tau \alpha_1^*(t-\tau)[L, \rho_s(t)L(\tau - t)^\dagger] + O(g^3),\end{aligned} \tag{21}$$

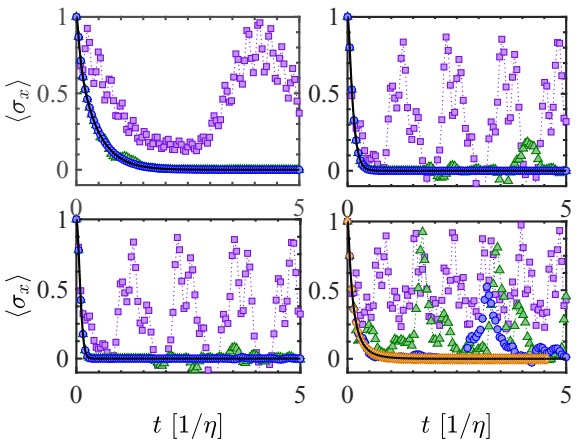

FIG. 2. (Color online) Evolution of the mean value of $\langle\sigma_x(t)\rangle$ for $a = b = 1/\sqrt{2}$ for $\eta = 0.1$ and $\omega_S = 0$. The top panels correspond to the Ohmic model ($s = 1$) for $\beta = 5$ (left) and $\beta = 1$ (right). The bottom panels correspond to a sub-Ohmic model with $s = 1/2$ (left) and a super-Ohmic model with $s = 3/2$ (right), both for $\beta = 1$. The exact solution is given by the solid black curves. For the MPS, we consider a varying M: purple, green, and blue curves with purple squares, green triangles, and blue circles correspond to $M = 2, 10, 40$ respectively, in all plots. The last plot includes a curve with orange diamonds with $M = 120$. Bond dimension is $D = 20$, and maximum occupation numbers in the harmonic oscillator basis is $n = 3$.

with $\alpha_1(t-\tau) = \sum_k g_k^2(n_k + 1)e^{-i\omega_k(t-\tau)}$, $\alpha_2(t-\tau) = \sum_\lambda g_k^2 n_k e^{i\omega_k(t-\tau)}$, and $L(t) = e^{iH_S t} L e^{-iH_S t}$.

To derive this equation, the Born approximation has also been assumed. This ME neglects the system-environment correlations and considers that the latter remains in the thermal equilibrium state ρ_B during the interaction, so that $\rho_{\mathrm{tot}}(t) \approx \rho_s(t) \otimes \rho_B$.

As shown in Fig. 3, the ME and the MPS coincide quite reasonably at weak couplings. However, as shown in Fig. 4, for stronger couplings the ME does not give an accurate description of the dynamics. Indeed, the MPS results describe comparatively a much slower decay for the two

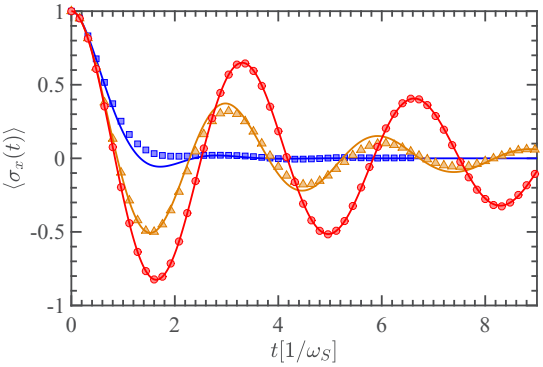

FIG. 3. (Color online) Comparison of ME (solid curves) with MPS results for $\langle\sigma_x(t)\rangle$ considering $\eta = 0.01$, $\omega_S = 0.1$, and $M = 100$ for both chains. We consider $\beta = 10$ (blue squares), $\beta = 50$ (orange triangles) and $\beta = 1000$ (red circles). We observe that the MPS results are converged with maximum population per oscillator $n = 4$.

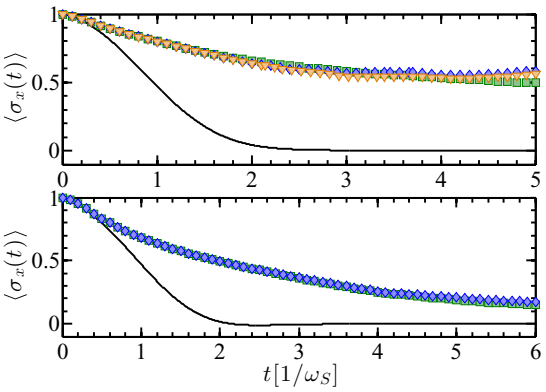

FIG. 4. (Color online) Evolution of $\langle\sigma_x(t)\rangle$ for (top) $\beta = 10$ (with maximum bond dimension $D = 40$) and (bottom) $\beta = 50$ (with $D = 20$) for $\eta = 0.1$, $\omega_S = 0.1$, and $M = 100$ for both chains. The solid black curve corresponds to the solution for the ME. Considering n_1 the dimension of the first two oscillators in the chain and n_2 the dimension of the following ones, the curves with green squares correspond to $(n_1 = 5, n_2 = 4)$, and the ones with blue diamonds correspond to $(n_1 = 6, n_2 = 5)$ (bottom panel) and $(n_1 = 7, n_2 = 6)$ (top panel). The curve with orange triangles in the top panel corresponds to $(n_1 = 8, n_2 = 7)$.

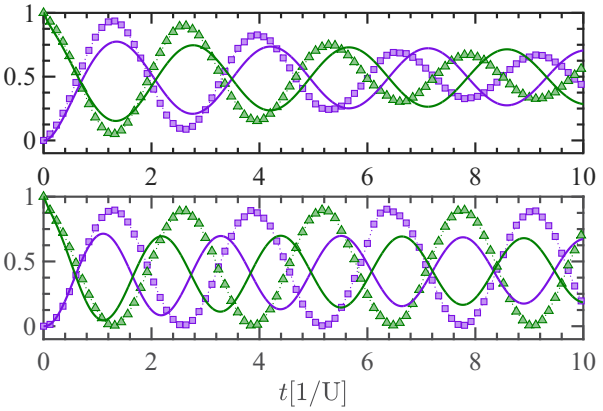

FIG. 5. (Color online) Evolution of $\langle n_\uparrow\rangle$ (green triangles) and $\langle n_\downarrow\rangle$ (purple squares) for the ME (solid lines) and the t-DMRG (symbols). We have considered (top) $\beta = 1$ and (bottom) $\beta = 10$ with $U = 0.2$, $V = -U/2$, $\omega_c = 15$, $t = 0.01$, and $M = 100$ oscillators in the chain.

temperature values considered here. Also, the computational cost of the MPS in the strong-coupling regime is much higher than at weak coupling. Nevertheless, the difference of the present scheme is that the excitations involved in the numerical resolution are just those that are dynamically generated due to the interaction with the OQS. This is in clear contrast to traditional methods in which the initial state of the environment is thermal, and therefore, it already has a finite initial occupation in the environment basis.

B. A quantum dot coupled to an electronic reservoir

As noted above, our proposal is valid also for fermionic environments. To illustrate this, we consider the Anderson impurity model [47], which constitutes one of the most relevant basis models in condensed matter [15,48,49] and quantum chemistry [50]. The model describes a quantum dot (QD) coupled to an electronic reservoir at a finite temperature with a Hamiltonian $H = H_S + H_B + H_{hy}$. Here,

$$H_S = \sum_\sigma \left(V n_\sigma + \frac{U}{2} n_\sigma n_{\bar\sigma} \right) \tag{22}$$

is the Hamiltonian of the quantum dot, which is represented using the Anderson impurity model with an on-site Coulomb repulsion U and an on-site energy V. In addition, the operator $n_\sigma = d_\sigma^\dagger d_\sigma$ measures the number of electrons with spin $\sigma = \uparrow, \downarrow$ at the dot. We consider that the QD is connected to the reservoir through a hybridization term

$$H_{hy} = -t \sum_{k;\sigma} g_k (d_\sigma^\dagger b_k + \text{H.c.}), \tag{23}$$

which is a sum of bilinear terms wherein $d_{i\sigma}^\dagger$ $(d_{i\sigma})$ creates (annihilates) an electron at the dot with spin σ and $b_k^\dagger$ (b_k) creates (annihilates) an electron with arbitrary spin and momentum k in the reservoir. Hence, the interaction Hamiltonian has a form similar to the one in (1), but redefining $L = -t \sum_\sigma d_\sigma$. For simplicity, we have considered that both spins σ couple equally to the reservoir. The Hamiltonian of the environment is $H_B = \sum_k \omega_k b_k^\dagger b_k$.

After the thermofield transformation, the former Hamiltonian is written in terms of $\tilde H_B = \sum_k \omega_k (a_{1k}^\dagger a_{1k} - a_{2k}^\dagger a_{2k})$ and an interaction Hamiltonian of the form (5) with couplings $g_{1k} = -t g_k \sqrt{1 + f_k}$ and $g_{2k} = -t g_k \sqrt{f_k}$, with $f_k = [1 + \exp(\beta\omega_k)]^{-1}$. We consider a spectral density of sub-Ohmic type, with $s = 0.5$ in Eq. (19).

Comparing the MPS results to those of the ME, as shown in Fig. 5, we find initial agreement, as expected, but then the results start to differ considerably even at relatively weak couplings. Due to the limited size of the fermionic basis, the MPS converges to the exact result with relatively small computational resources.

V. CONCLUSIONS AND OUTLOOK

Based on a thermofield approach, our formalism allows us to efficiently integrate the dynamics of an OQS coupled to a thermal reservoir, either bosonic or fermionic, in a pure-state formalism, without previously preparing the thermal state with imaginary-time evolution. The approach is based on performing an analytical (thermal Bogoliubov) transformation over the (physical) environment and an auxiliary one. Provided the thermal state of the original environment is known, more concretely, that the quantities n_k can be analytically or numerically computed, our approach can be used to solve thermalization problems of OQS using only zero-temperature (pure-state) MPS.

ACKNOWLEDGMENTS

We thank D. Alonso, U. Schollwöck, F. Heidrich-Meisner, and C. A. Büsser for helpful discussions. This work was supported by Nanosystems Initiative Munich (NIM; Project No. 862050-2) and partially by the Spanish MICINN (Grant No. FIS2013-41352-P) and the EU through a SIQS grant (FP7 600645).

APPENDIX: NUMERICAL METHOD

The thermofield transformation described in this paper can be used in combination with any method to solve one-dimensional problems. Particularly suited are, nevertheless, methods based on the matrix product state (MPS) approximation. Although extensive literature exists about these methods (see, e.g., [25,26]), for the sake of completeness, we compile in this Appendix the main ingredients of the approach used for our numerical results.

A MPS for a system of N sites with finite physical dimensions $d_1, d_2, \ldots, d_N$, is a state of the form

$$|\Psi\rangle = \sum_{i_1}^{d_1} \sum_{i_2}^{d_2} \cdots \sum_{i_N=1}^{d_N} \mathrm{tr}\left(A_1^{i_1} \cdots A_N^{i_N}\right) |i_1, \ldots, i_N\rangle, \qquad \text{(A1)}$$

where $\{|i_k\rangle\}_{i=0}^{d_k-1}$ is the local basis of site k. A_k^i are D-dimensional matrices, whose dimension D, known as bond dimension, determines the number of parameters in the ansatz. The MPS ansatz is extremely successful for the approximation of ground states and low-lying excitations of local Hamiltonians [27,51], and it can also be used to simulate real-time evolution [24,52], such as that required by the problem we discuss.

To explore the potential of the thermofield representation, we have applied the MPS ansatz to the global state of the system plus the double chain that represents the vacuum. The whole system has the geometry of a chain, with nearest-neighbor hopping terms among modes C_n and B_n, on the left and right of the central site that represents the two-level system, respectively. Although the exact mapping introduces semi-infinite chains of B and C modes, we can truncate them to a finite length N. This allows us to reliably study the evolution until finite-size effects appear. An analysis of the truncation error bounds and the optimality of the present chain representation have been recently derived in [23,53]

Dealing with bosonic degrees of freedom requires the truncation of the physical dimension of each bosonic mode in order to keep the local physical dimensions finite and to allow the application of the MPS ansatz. Although more sophisticated methods exist [54], we observe that in our case simply truncating the maximum occupation number of each bosonic mode to $n_{\max} = 3 - 8$ suffices to observe convergence in our simulations. This can be explained by the fact that the initial state we consider is the vacuum of all bosonic modes and the only excitations injected in the bath are the ones coming from the system, so that states where some bosonic mode is highly occupied make only a small contribution to the physical states that we want to describe.

In the case of a fermionic system, the truncation of the bath modes is not necessary, as these modes are represented exactly with a local basis of dimension 2. In particular, in that case we apply a Jordan-Wigner transformation [55] to map the fermionic system to a spin chain. In this case, we consider a system with two fermionic modes (e.g., a fermion with spin), which can be represented as a central site with dimension 4 in our chain.

The initial state in our problem, i.e., the vacuum of the thermofield representation, is simply a tensor product of the vacuum for each individual mode times the initial state of the system and thus has an exact MPS representation with bond dimension $D = 1$.

To simulate the time evolution of the full system, we use standard tensor network techniques [24,28], in which the time evolution operator, $U = \exp(-iHt)$, is approximated by dividing the total time in small steps δ. In order to evolve the MPS ansatz, for each step the corresponding evolution operator needs to be approximated by a MPO [56]. This is achieved in our case by a fourth-order Suzuki-Trotter decomposition [57], in which the Hamiltonian is written as a sum of even and odd terms. The exponential of the sum is then approximated as a product of several exponentials of the individual terms, which have exact MPO expressions [56]. The action of each of these MPOs on the MPS state is approximated by a new MPS. Since the exact application of the MPO would, in general, make the bond dimension of the state grow, the resulting MPS needs to be truncated to the maximum allowed bond dimension D. We do this using a global optimization, as introduced in [28], and iterate the procedure until the desired time is reached.

This method has different sources of error, each controlled by a truncation parameter. In general, the precision of the results can be estimated by computing and comparing results with different parameters until sufficient convergence is found.

First of all, the truncation of the thermofield mapping to finite chains of length N introduces a finite-size effect. Since we are interested in the dynamics of the system and thus look at only local observables in the center of the complete chain, such effects will appear only after long times, and we find that taking $N \approx 100$ suffices to determine the behavior of the system in all cases of interest.

Second, the discrete time step δ in the Suzuki-Trotter decomposition corresponds to applying an approximation of the evolution operator, instead of the exact one. This error, however, only grows linearly with time, and it is easily reducible by using a higher-order Suzuki-Trotter expansion, as we do here.

Finally, the maximum bond dimension used in the numerical simulations D introduces a truncation error.

In our study, we run the simulations using different values of D and estimate the error by comparing the corresponding results. As mentioned above, in the case of bosonic baths, there is an additional truncation parameter given by the maximum occupation allowed for bosonic modes. The results presented in this paper correspond to choices of parameters such that the errors coming from all these sources are much smaller than the effects we want to discuss.

[1] H. Breuer and F. Petruccione, *The Theory of Quantum Open Systems* (Oxford University Press, Oxford, 2002).

[2] A. Rivas and S. F. Huelga, *Open Quantum Systems: An Introduction* (Springer, Heidelberg, 2011).

[3] L. Diósi, N. Gisin, and W. T. Strunz, Phys. Rev. A **58**, 1699 (1998).

[4] T. Yu, Phys. Rev. A **69**, 062107 (2004).

[5] D. Alonso and I. de Vega, Phys. Rev. Lett. **94**, 200403 (2005).

[6] M. Plenio and P. Knight, Rev. Mod. Phys. **70**, 101 (1998).
[7] J. Piilo, K. Härkönen, S. Maniscalco, and K.-A. Suominen, Phys. Rev. A **79**, 062112 (2009).
[8] D. Walls and G. Milburn, *Quantum Optics* (Springer, Berlin, 1994).
[9] L. Mühlbacher and J. Ankerhold, J. Chem. Phys. **122**, 184715 (2005).
[10] C. Zhang, E. Jeckelmann, and S. R. White, Phys. Rev. Lett. **80**, 2661 (1998).
[11] J. Bonča, S. A. Trugman, and I. Batistić, Phys. Rev. B **60**, 1633 (1999).
[12] L. Vidmar, J. Bonča, and S. A. Trugman, Phys. Rev. B **82**, 104304 (2010).
[13] K. G. Wilson, Rev. Mod. Phys. **47**, 773 (1975).
[14] M. Vojta, N.-H. Tong, and R. Bulla, Phys. Rev. Lett. **94**, 070604 (2005).
[15] R. Bulla, T. A. Costi, and T. Pruschke, Rev. Mod. Phys. **80**, 395 (2008).
[16] F. B. Anders, R. Bulla, and M. Vojta, Phys. Rev. Lett. **98**, 210402 (2007).
[17] A. Weichselbaum and J. von Delft, Phys. Rev. Lett. **99**, 076402 (2007).
[18] K. Hughes, C. Christ, and I. Burghardt, J. Chem. Phys. **131**, 024109 (2009).
[19] H. R. Krishna-murthy, J. W. Wilkins, and K. G. Wilson, Phys. Rev. B **21**, 1003 (1980).
[20] J. Prior, A. W. Chin, S. F. Huelga, and M. B. Plenio, Phys. Rev. Lett. **105**, 050404 (2010).
[21] A. W. Chin, A. Rivas, S. F. Huelga, and M. B. Plenio, J. Math. Phys. **51**, 092109 (2010).
[22] A. W. Chin, S. F. Huelga, and M. B. Plenio, in *Semiconductors and Semimetals*, edited by U. Wurfel, M. Thorwart, E. R. Weber, and C. Jagadish (Academic, Amsterdam, 2011), pp. 115–144.
[23] I. de Vega, U. Schollwöck, and F. A. Wolf, Phys. Rev. B **92**, 155126 (2015).
[24] G. Vidal, Phys. Rev. Lett. **91**, 147902 (2003).
[25] F. Verstraete, V. Murg, and J. Cirac, Adv. Phys. **57**, 143 (2008).
[26] U. Schollwöck, Ann. Phys. (N.Y.) **326**, 96 (2011).
[27] U. Schollwöck, Rev. Mod. Phys. **77**, 259 (2005).
[28] F. Verstraete, J. J. García-Ripoll, and J. I. Cirac, Phys. Rev. Lett. **93**, 207204 (2004).
[29] M. Zwolak and G. Vidal, Phys. Rev. Lett. **93**, 207205 (2004).
[30] V. Bargmann, Commun. Pure Appl. Math. **14**, 187 (1961).
[31] H. Araki and E. J. Woods, J. Math. Phys. **4**, 637 (1963).
[32] Y. Takahashi and H. Umezawa, Collect. Phenom. **2**, 55 (1975).
[33] M. Blasone, P. Jizba, and G. Vitiello, *Quantum Field Theory and Its Macroscopic Manifestations Boson Condensation, Ordered Patterns and Topological Defects* (World Scientific, Singapore, 2011).
[34] J. Maldacena and L. Susskind, Fortschritte der Physik **61**, 781 (2013).
[35] W. Israel, Phys. Lett. A **57**, 107 (1976).
[36] W. Gautschi, J. Comput. Appl. Math. **178**, 215 (2005).
[37] B. Bruognolo, A. Weichselbaum, C. Guo, J. von Delft, I. Schneider, and M. Vojta, Phys. Rev. B **90**, 245130 (2014).
[38] A. J. Leggett, S. Chakravarty, A. T. Dorsey, Matthew P. A. Fisher, A. Garg, and W. Zwerger, Rev. Mod. Phys. **59**, 1 (1987).
[39] U. Weiss, in *Quantum Dissipative Systems*, Series in Modern Condensed Matter Systems (World Scientific, Singapore, 2008), pp. 27–28.
[40] M. Florescu and S. John, Phys. Rev. A **64**, 033801 (2001).
[41] I. de Vega, D. Alonso, and P. Gaspard, Phys. Rev. A **71**, 023812 (2005).
[42] Q. Si, S. Rabello, K. Ingersent, and J. L. Smith, Nature (London) **413**, 804 (2001).
[43] A. Shnirman, Y. Makhlin, and G. Schön, Phys. Scr. **2002**, 147 (2002).
[44] N.-H. Tong and M. Vojta, Phys. Rev. Lett. **97**, 016802 (2006).
[45] C. Seoanez, F. Guinea, and A. H. C. Neto, Europhys. Lett. **78**, 60002 (2007).
[46] D. Alonso and I. de Vega, Phys. Rev. A **75**, 052108 (2007).
[47] P. W. Anderson, Phys. Rev. **124**, 41 (1961).
[48] F. Heidrich-Meisner, A. E. Feiguin, and E. Dagotto, Phys. Rev. B **79**, 235336 (2009).
[49] A. Holzner, I. P. McCulloch, U. Schollwöck, J. von Delft, and F. Heidrich-Meisner, Phys. Rev. B **80**, 205114 (2009).
[50] D. Zgid and G. K.-L. Chan, J. Chem. Phys. **134**, 094115 (2011).
[51] S. R. White, Phys. Rev. Lett. **69**, 2863 (1992).
[52] A. J. Daley, C. Kollath, U. Schollwöck, and G. Vidal, J. Stat. Mech. (2004) P04005.
[53] M. P. Woods and M. B. Plenio, arXiv:1508.07354.
[54] C. Guo, A. Weichselbaum, J. von Delft, and M. Vojta, Phys. Rev. Lett. **108**, 160401 (2012).
[55] P. Jordan and E. Wigner, Z. Phys. **47**, 631 (1928).
[56] B. Pirvu, V. Murg, J. I. Cirac, and F. Verstraete, New J. Phys. **12**, 025012 (2010).
[57] M. Suzuki, Proc. Jpn. Acad. **69**, 161 (1993).